Proton and Carbon tracking in an Ion Rapid Cycling Medical Synchrotron

D. T. Abell, D. L. Bruhwiler, N. M. Cook — RadiaSoft LLC, Boulder, CO
S. Peggs, D. Trbojevic, F. Méot — Brookhaven National Lab, Upton, NY
V. L. Bailey, M. Subramanian — Best Medical, Springfield, VA
J. Lidestri — Best Medical, Springfield, VA & Columbia University, NY, NY

Abstract

A low-energy ion rapid-cycling medical synchrotron (iRCMS) is under development for proton- and carbon-ion therapy applications [4]. In the current design, the two main arcs comprise six girders, each of which holds a pair of FODO cells formed by a set of combined-function magnets. The field overlap between the combined-function bending magnets is such that accurate simulations require treating the entire girder as a single magnetic unit. We describe and present results from simulations using PTC [1] and Zgoubi [2, 3] to study this machine.

The iRCMS

The ion Rapid-Cycling Medical Synchrotron (iRCMS) pictured here is designed to operate at 15 Hz and accelerate either protons or fully-stripped carbon ions from 8 MeV/u up to a maximum energy of 206 MeV/u for p^+, or 400 MeV/u for C^{6+}.

The two straight sections accommodate injection, extraction, and rf acceleration. The remaining portion of the lattice is contained in a set of six 60°-girders, each of which comprises a pair of FODO cells with combined-function bending magnets separated by small drifts. Initial simulations of any given design are performed using the standard combined-function bend elements in available in MAD-X, PTC, and Zgoubi. For robust analyses, however, it is essential to perform detailed integration that includes the effect of overlapping fringe fields.

Lattice Functions

We have used MAD-X to simulate various versions of the iRCMS lattice. Our initial simulations were of the original BNL design for C^{6+} ions at both injection and extraction. Those simulations confirmed results obtained during the initial design phase. In particular, we obtained the following lattice functions for C^{6+} ions at injection:

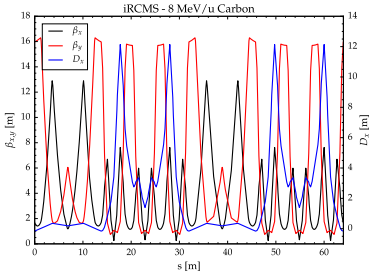

The original design included limited space for the necessary rf cavities. We therefore explored the possibility of increasing the space allotted to 3.5 m. In this effort we made no modifications to the arc; only the drift lengths and quadrupole strengths of the long straight sections were adjusted. In addition, the total length of the lattice was constrained to remain at the original design value of 64 m. Here are the updated lattice functions for C^{6+} ions at injection:

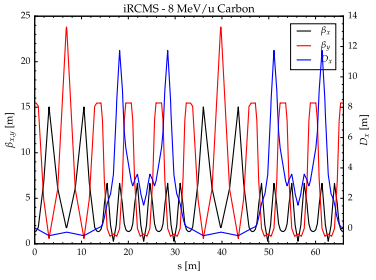

The principal differences in the betatron functions are the increases in the maxima: from 13 m to 15 m for β_x, and the more significant 50 % increase from about 16 m to about 24 m for β_y. A subtler—but also significant—difference is that the absolute maximum in the horizontal dispersion in the "dispersion-free" straight section has risen from about 0.35 to about 0.50. We must point out that the dispersion shown here uses the new MAD-X convention, which defines dispersion in terms of relative *energy* deviation rather than relative *momentum* deviation. To convert to the traditional definition at these energy values, it suffices to multiply by the normalized velocity $\beta \approx 0.13$. In other words, the absolute dispersion defined on the basis of $\delta = \Delta p/p$ have maxima of about 0.046 and 0.065 respectively in the original and new designs.

Girder Magnetic Field

We received from the magnet manufacturer, Everson-Tesla, several sets of OPERA simulation data that describe in detail the magnetic field within a single girder, extending about 6° on either end to cover the fringe field region. The mesh had a resolution of about 3 mm in each direction. Here is the data along the central arc:

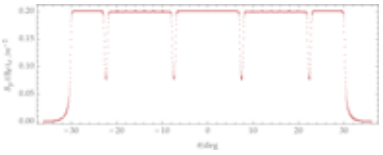

The goal is to use the magnet field data for detailed tracking studies using either Zgoubi or PTC. Zgoubi has built-in capabilities for reading OPERA and TOSCA output. PTC, on the other hand requires two significant transformations of the data: (i) rotate the fields at each position into PTC's local frame of reference; (ii) fit each of the field components B_x, B_y, and B_z in a single azimuthal slice—*i.e.* a plane orthogonal to the beam direction—to a truncated Taylor series in the transverse variables. We used a 6th-order Taylor series for the latter transformation.

In the course of analyzing the girder field data, we computed the quadrupole strength $g = \mathrm{d}B_y/\mathrm{d}x$ along the central arc. We also determined the magnetic rigidity of the beam corresponding to the given field data as

$$(B\rho)_o = \frac{1}{\theta_o}\int B_y(s)\,\mathrm{d}s = \frac{1}{\pi/3}\int B_y(s)\,\mathrm{d}s \approx 3.3658.$$

Scaling the gradient g by this estimate of $(B\rho)_o$, we obtained k_1, the scaled quadrupole field strength along the girder's central arc:

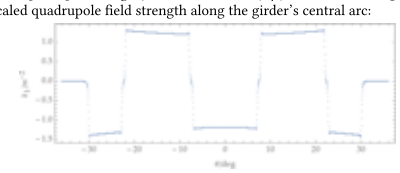

The following three graphics show contour levels of k_1 in the three distinct sectors of girder magnet data.

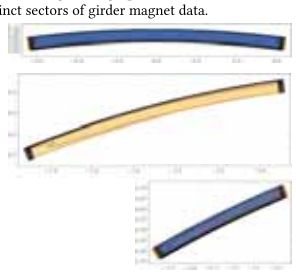

sector BD

sector BF

sector BDH

Using the minima in B_y as separation points, we also integrated k_1 within each of the girder's five sectors to obtain the values

$$k_1 L \equiv \int_{\text{sector}} k_1\,\mathrm{d}s = \{-0.8862,\ +1.5646,\ -1.5067,\ +1.5646,\ -0.8862\}\ \mathrm{m}^{-1}$$

for the integrated quadrupole strengths of the individual girder magnets. These strengths, however, differ significantly from the values

$$k_1 L = \{-0.8946,\ +1.8050,\ -1.8041,\ +1.8050,\ -0.8946\}\ \mathrm{m}^{-1}$$

in the original BNL lattice design: The outer pair of values are in reasonable agreement; whereas for the inner trio, the values obtained from the magnet simulation are of order 15 % lower than those called for in the original design.

Tracking simulations

Using Zgoubi, we identified an appropriate reference trajectory through the arc: We first added a half-drift at each end of the field map to account for the separation drift between adjacent 60° sectors. We then identified the reference trajectory by constraining it to (a) enter and exit normal to the "faces" of the 60° sector, and (b) have identical entrance and exit radii in the frame of the field map.

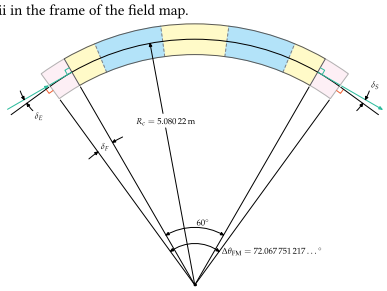

To achieve this, we adjusted the field amplitude and the radial position of the field map. Zgoubi reports the field profile along this trajectory, as shown in the following graph:

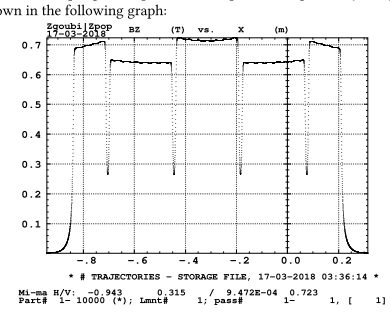

The small ripples seen above reflect actual ripples in the magnetic field. These are a consequence of how laminated segments are oriented in the process of assembling this magnet.

For the corresponding transport matrix about that reference trajectory, Zgoubi reports the following:

```
-1.19631  -1.07306   0.00000   0.00000   0.00000   1.16030
-0.39040  -1.18072   0.00000   0.00000   0.00000   0.20757
 0.00000   0.00000  -1.03907   1.03142   0.00000   0.00000
 0.00000   0.00000   0.07723  -1.03906   0.00000   0.00000
 0.20480   1.16464   0.00000   0.00000   1.00000   0.69162
 0.00000   0.00000   0.00000   0.00000   0.00000   1.00000
```

Such a system is *not* stable: $|\mathrm{Tr}(\mathrm{matrix})| > 2$ in both transverse planes.

Because of the significant differences identified between the design gradients in the arcs and the values derived from the magnet simulation, we also performed simulations using standard elements set with those derived gradient values. Those simulations, whether in MAD-X, PTC, or Zgoubi, yield unstable lattices. Efforts to stabilize the design by adjusting the straight-section quadrupoles yield unsatisfactory lattices.

If the simulated magnet faithfully represents the built magnet, then the current girder will have to be dismantled, it's pole faces reshaped, and then the girder reassembled.

References

[1] É. Forest, F. Schmidt, and E. McIntosh. Introduction to the Polymorphic Tracking Code. KEK Report 2002-3, KEK, Tsukuba, Japan, 2002.

[2] F. Méot. Zgoubi. `http://sourceforge.net/projects/zgoubi/`.

[3] F. Méot. Zgoubi users' guide. Technical Report FERMILAB-TM-2010, Fermi National Accelerator Laboratory, Batavia, IL, Oct. 1997.

[4] D. Trbojevic et al. Lattice design of a rapid cycling medical synchrotron for carbon/proton therapy. In *Proc. IPAC'11*, pages 2541–2543, 2011.